JOURNAL OF THERMOPHYSICS AND HEAT TRANSFER
Vol. 15, No. 3, July–September 2001

Verification and Validation of Adaptive Finite Element Method for Impingement Heat Transfer

É. Turgeon* and D. Pelletier†
École Polytechnique de Montréal, Montréal, Québec H3C 3A7, Canada

Aadaptive finite element computations of laminar and turbulent jet impingement heat transfer are presented. Turbulence is modeled using the standard k–ϵ model for high Reynolds number, coupled with wall functions. The turbulence model is solved in logarithmic form. The error estimator uses a local least-squares projection of derivatives and accounts for errors in all dependent variables, including the eddy viscosity. The performance of the methodology is verified by solving a problem possessing a closed-form solution. Two applications are then considered: laminar and turbulent impinging jets. In both cases heat transfer is a key element of the study. Results indicate that the methodology produces grid-independent solutions even for derived quantities in thin boundary layers. Emphasis is put on these accuracy verifications. Numerical predictions are compared to experimental data to validate the flow models.

Nomenclature

C_f	=	skin-friction coefficient
C_p	=	pressure coefficient
$C_{\epsilon 1}$, $C_{\epsilon 2}$, C_μ, σ_k, σ_ϵ	=	k–ϵ model constants
c_p	=	specific heat at constant pressure
d	=	pipe diameter
E	=	roughness parameter
$\mathcal{E}$	=	natural logarithm of ϵ
$\mathcal{K}$	=	natural logarithm of k
k	=	turbulence kinetic energy
L	=	pipe exit height above plate
Nu	=	Nusselt number
Pr	=	Prandtl number
p	=	pressure
q_w	=	wall heat flux
q''	=	imposed wall heat flux
Re	=	Reynolds number
St	=	Stanton number
T	=	temperature
U	=	reference velocity
$\boldsymbol{u}$	=	velocity
u, v	=	velocity components
x, r	=	cylindrical coordinates
y	=	distance to the wall
ϵ	=	turbulence dissipation rate
κ	=	Kármán constant
λ	=	thermal conductivity
μ	=	viscosity
ρ	=	density
τ_w	=	wall shear stress

Subscripts

i	=	from the preceding iteration
T	=	turbulent
t	=	tangent to the wall
w	=	at the boundary or at the wall
z	=	normal to the wall
$+$	=	dimensionless (wall functions)
∞	=	freestream value

Received 7 April 2000; revision received 12 December 2000; accepted for publication 20 December 2000.

*Graduate Student, P.O. Box 6079, Mechanical Engineering Department, Station Centre-ville.

†Professor, P.O. Box 6079, Mechanical Engineering Department, Station Centre-ville. Associate Fellow AIAA.

Introduction

IMPINGING round jets are widely used in industry. The very high heat transfer coefficients they generate make them particularly attractive for cooling, drying, and heating operations. Turbulent jets are more frequently encountered and have received more attention from the scientific community. Both laminar and turbulent jets are considered with a focus on heat transfer predictions. However, flow predictions are also considered because they affect heat transfer.

The diversity of behaviors exhibited by impinging jets makes them interesting for a numerical study. They contain thin boundary and shear layers, impingement regions, free and wall jets, stagnation points, streamline curvature, heat transfer, and so on. Such a diversity constitutes a demanding test for computational heat transfer codes and especially for adaptive methods.

As already reported,[1–4] predictions by different authors for a given problem are sometimes quite different. The sometimes surprising scatter in the results is caused by a combination of elements: mathematical model, geometry and boundary conditions, mesh, numerical scheme, and so on. Often, authors report results from a single structured mesh computation without performing any grid-refinement studies. The accuracy of their predictions cannot be assessed. The objective of the present paper is to control and maximize the accuracy of the solution so as to obtain numerically exact solutions to the differential equations. With systematic adaptive grid refinement discretization errors become negligible. The differences between the numerical results and the experimental measurements are thus a matter of modeling. Validation of the turbulence models, for instance, may be performed rigorously on that basis.

Impinging jets constitute a particularly attractive test case for validation of turbulence models. In fact, the performance of the k–ϵ model of turbulence is known to be poor for this problem. Behnia et al.[5] and Craft et al.[6] report that heat transfer and the turbulence kinetic energy are widely overpredicted in the impingement region, when using a low-Reynolds-number k–ϵ model. Behnia et al. propose to use a tailored turbulence model V2F and show improved behavior for this specific application. Also, wall functions were not especially developed for impinging flows. However, some authors obtained reasonable heat-transfer predictions using the standard k–ϵ model with wall functions,[3] but no grid-refinement studies were reported. Despite its anticipated weakness, we choose to use the simpler standard k–ϵ model with wall functions. This choice will demonstrate the capability of the adaptive strategy to perform systematic verifications, thus allowing a rigorous validation of the

turbulence model for this type of flow. We will confirm/infirm the trends observed by other authors.

Adaptive methods provide a powerful approach to achieve such levels of accuracy especially for complex problems. The error estimator provides a quantification of the error, and the adaptive strategy becomes a simple means of verifying grid convergence. The adaptive methodology presented in this paper was previously applied with success to the k–ϵ model,[7,8] the k–ω model,[9,10] laminar and turbulent heat transfer,[1,11–16] and compressible turbulent flows.[17]

The paper is organized as follows. First, the modeling aspects are presented: the Reynolds and energy equations, turbulence model, and wall functions. The logarithmic variable approach for positivity preservation is then reviewed. It is followed by a summary of the finite element algorithm. Next, the adaptive methodology and error estimator are presented. The first computational results presented are those of a verification exercise: a grid-refinement study on a problem possessing a closed-form solution. The adaptive methodology is then applied to laminar and turbulent impinging jets. The paper ends with conclusions.

Modeling of the Problem

Reynolds-Averaged Navier–Stokes Equations

The flow regime of interest is modeled by the Reynolds-averaged Navier–Stokes equations:

$$\nabla \cdot \boldsymbol{u} = 0$$

$$\rho \boldsymbol{u} \cdot \nabla \boldsymbol{u} = -\nabla p + \nabla \cdot \left\{ (\mu + \mu_T)[\nabla \boldsymbol{u} + (\nabla \boldsymbol{u})^T] \right\} + \boldsymbol{f}$$

$$\rho c_p \boldsymbol{u} \cdot \nabla T = \nabla \cdot [(\lambda + \lambda_T) \nabla T] + q_s$$

where $\boldsymbol{f}$ is a body force and q_s is a heat source. The turbulent viscosity μ_T is computed using the k–ϵ model of turbulence. The turbulent conductivity λ_T is computed as

$$\lambda_T = c_p \mu_T / Pr_T$$

where the turbulent Prandtl number Pr_T is equal to unity. The system of equations is closed by including transport equations for the turbulence quantities.

Standard k–ϵ Model

For this model the turbulence quantities are the turbulence kinetic energy k and its dissipation rate ϵ, which are governed by the following transport equations[18]:

$$\rho \boldsymbol{u} \cdot \nabla k = \nabla \cdot [(\mu + \mu_T / \sigma_k) \nabla k] + \mu_T P(\boldsymbol{u}) - \rho \epsilon$$

$$\rho \boldsymbol{u} \cdot \nabla \epsilon = \nabla \cdot [(\mu + \mu_T / \sigma_\epsilon) \nabla \epsilon] + C_{\epsilon 1} (\epsilon / k) \mu_T P(\boldsymbol{u}) - C_{\epsilon 2} \rho (\epsilon^2 / k)$$

where the production of turbulence is defined as

$$P(\boldsymbol{u}) = \nabla \boldsymbol{u} : [\nabla \boldsymbol{u} + (\nabla \boldsymbol{u})^T]$$

The eddy viscosity is computed from k and ϵ by

$$\mu_T = \rho C_\mu (k^2 / \epsilon)$$

The constants σ_k, σ_ϵ, $C_{\epsilon 1}$, $C_{\epsilon 2}$, C_μ take on the standard values proposed by Launder and Spalding[18]:

$$\sigma_k = 1.0, \qquad \sigma_\epsilon = 1.3$$

$$C_{\epsilon 1} = 1.44, \qquad C_{\epsilon 2} = 1.92, \qquad C_\mu = 0.09$$

Wall Boundary Conditions

On a solid wall a combination of Neumann and Dirichlet conditions are imposed through wall functions, which describe the asymptotic behavior of the different variables near a solid boundary.[18] The normal derivative of the turbulence kinetic energy (TKE) is set to zero near the wall. Thus, the TKE values at boundary points k_w are computed implicitly. A mixed boundary condition for the momentum equations relates the wall shear stress τ_w to the tangential velocity at the boundary u_t:

$$\tau_w = u_t \left(\rho C_\mu^{\frac{1}{4}} k_w^{\frac{1}{2}} \right) \Big/ u^+$$

where

$$u^+ = \begin{cases} y^+ & \text{for} \quad y^+ < y_c^+ \\ (1/\kappa)\, \ell n(E y^+) & \text{for} \quad y^+ \geq y_c^+ \end{cases}$$

$$y^+ = \rho C_\mu^{\frac{1}{4}} k_w^{\frac{1}{2}} y / \mu$$

Here $E = 9.0$ for smooth walls. The normal velocity is set to zero.

Boundary conditions at a wall for the energy equation are enforced by a temperature wall function similar to that used for the momentum equations. If a constant heat flux q'' is imposed, a classical natural boundary condition is used: $q_w = q''$. Otherwise, if the wall is at a constant temperature, the effective heat flux in the wall function is computed as

$$q_w = \left[\rho c_p C_\mu^{\frac{1}{4}} k_w^{\frac{1}{2}} (T - T_w) \Big/ T^+ \right]$$

where T_w is the wall temperature and T^+ satisfies the following relations[19]:

$$T^+ = \begin{cases} Pr y^+ & \text{for} \quad y^+ < y_1^+ \\ a_2 - \dfrac{Pr_T}{2 a_1 (y^+)^2} & \text{for} \quad y_1^+ \leq y^+ < y_2^+ \\ \dfrac{Pr_T}{\kappa}\, \ell n(y^+) + \beta & \text{for} \quad y_2^+ \leq y^+ \end{cases}$$

with the following definitions:

$$y_1^+ = 10 \Big/ Pr^{\frac{1}{3}}, \qquad y_2^+ = (\kappa / a_1)^{\frac{1}{2}}$$

$$a_1 = 10^{-3} Pr_T, \qquad a_2 = 15 Pr^{\frac{2}{3}}$$

$$\beta = a_2 - Pr_T / 2\kappa [1 + \ell n(\kappa / a_1)]$$

Finally, the turbulence dissipation rate at boundary points is computed as follows:

$$\epsilon_w = C_\mu^{\frac{3}{4}} k_w^{\frac{3}{2}} \Big/ \kappa y$$

Logarithmic Form of the Turbulence Equations

Although mathematically correct, the turbulence equations can cause numerical difficulties. For example, the eddy viscosity may become negative if ϵ becomes negative. This causes a dramatic breakdown of the solver. Also, several source terms contain division by a turbulence variable. Negative or small values of the denominator can cause improper sign or overly large values of the source terms. Enhanced robustness of the algorithm will be achieved if one can ensure that turbulence variables remain positive throughout the domain and the course of iterations.

One way to preserve positivity of the dependent variables consists in solving for their logarithms.[8,20] This can be viewed as using the following change of dependent variables:

$$\mathcal{K} = \ell n(k) \qquad \mathcal{E} = \ell n(\epsilon)$$

Solving for $\mathcal{K}$ and $\mathcal{E}$ guarantees that k and ϵ will remain positive throughout the computations. Hence, the eddy viscosity μ_T will always remain positive. This approach is referred to as solving for logarithmic variables. Furthermore, turbulence quantities often present very steep fronts that are difficult to solve accurately. Logarithmic variables $\mathcal{K}$ and $\mathcal{E}$ present smoother variations than those of k and ϵ because the logarithm varies more slowly than its argument. Thus, more accurate solutions are obtained when logarithmic variables are used.

The transport equations for the logarithmic variables are

$$\rho \boldsymbol{u} \cdot \nabla \mathcal{K} = \nabla \cdot [(\mu + \mu_T/\sigma_k)\nabla \mathcal{K}] + (\mu + \mu_T/\sigma_k)(\nabla \mathcal{K})^2 + \mu_T e^{-\mathcal{K}} P(\boldsymbol{u}) - \rho e^{\mathcal{E}-\mathcal{K}}$$

$$\rho \boldsymbol{u} \cdot \nabla \mathcal{E} = \nabla \cdot [(\mu + \mu_T/\sigma_\epsilon)\nabla \mathcal{E}] + (\mu + \mu_T/\sigma_\epsilon)(\nabla \mathcal{E})^2 + C_{\epsilon 1}\mu_T e^{-\mathcal{K}} P(\boldsymbol{u}) - C_{\epsilon 2}\rho e^{\mathcal{E}-\mathcal{K}}$$

The equations for logarithmic variables are equivalent to the original equations of the turbulence model. Hence, the turbulence model is unchanged. Only the computational variables are different.

Solution Algorithm

A robust finite element scheme is obtained by rewriting the equations for k and ϵ using the eddy viscosity definition.[7] Thus, ϵ can be rewritten as

$$\epsilon = \rho C_\mu \left(k^2/\mu_T\right)$$

to achieve the following block-triangular form of the turbulence equations:

$$\rho \boldsymbol{u} \cdot \nabla k = \nabla \cdot [(\mu + \mu_T/\sigma_k)\nabla k] + \mu_T P(\boldsymbol{u}) - \rho^2 C_\mu \left(k^2/\mu_T\right)$$

$$\rho \boldsymbol{u} \cdot \nabla \epsilon = \nabla \cdot [(\mu + \mu_T/\sigma_\epsilon)\nabla \epsilon] + \rho C_{\epsilon 1} C_\mu k P(\boldsymbol{u}) - C_{\epsilon 2}\rho(\epsilon^2/k)$$

After some algebra the following logarithmic form of the turbulence equations is obtained for implementation in the the finite element algorithm:

$$\rho \boldsymbol{u} \cdot \nabla \mathcal{K} = \nabla \cdot [(\mu + \mu_{\mathrm{Ti}}/\sigma_k)\nabla \mathcal{K}] + (\mu + \mu_{\mathrm{Ti}}/\sigma_k)(\nabla \mathcal{K})^2 + \mu_{\mathrm{Ti}} e^{-\mathcal{K}} P(\boldsymbol{u}) - \rho^2 C_\mu \left(e^{\mathcal{K}}/\mu_{\mathrm{Ti}}\right)$$

$$\rho \boldsymbol{u} \cdot \nabla \mathcal{E} = \nabla \cdot [(\mu + \mu_{\mathrm{Ti}}/\sigma_\epsilon)\nabla \mathcal{E}] + (\mu + \mu_{\mathrm{Ti}}/\sigma_\epsilon)(\nabla \mathcal{E})^2 + \rho C_{\epsilon 1} C_\mu e^{\mathcal{K}-\mathcal{E}} P(\boldsymbol{u}) - \rho C_{\epsilon 2} e^{\mathcal{E}-\mathcal{K}}$$

The eddy viscosity μ_T and its values at the preceding iteration μ_{Ti} are evaluated by

$$\mu_T = \rho C_\mu e^{2\mathcal{K}-\mathcal{E}}$$

$$\mu_{\mathrm{Ti}} = \rho C_\mu e^{2\mathcal{K}_i - \mathcal{E}_i}$$

The preceding equations are solved in a partly segregated manner using the following algorithm:

1) Given initial conditions $\boldsymbol{u}_i$, T_i, $\mathcal{K}_i$, and $\mathcal{E}_i$
2) Compute μ_{Ti} from $\mathcal{K}_i$ and $\mathcal{E}_i$
3) for μ_{Ti} given
   a) solve momentum, continuity and energy
   b) solve the $\mathcal{K}$ equation
   c) solve the $\mathcal{E}$ equation
   d) update μ_T and go to 3.

Subiterations of steps 3b–3d are also used to accelerate the overall convergence of the iterative process.

The preceding equations are completely equivalent to those presented in the preceding section even though some terms appear in a different form. These differences arise from the fact that, here, the k–ϵ system is written in upper triangular form before using logarithmic variables.

The Navier–Stokes and turbulence equations are solved by a finite element method. The equations are discretized using the seven-node triangular element,[21] which uses an enriched quadratic velocity field, a linear discontinuous pressure, and a quadratic interpolant for the logarithms of turbulence variables and for the temperature.

Adaptive Methodology

The adaptive remeshing procedure used here is modeled after that proposed by Peraire et al.[22] and is described in more details by Ilinca.[7,20] The procedure clusters grid points in regions of rapid variations of all dependent variables: velocity, pressure, temperature, logarithmic turbulence variables, and the eddy viscosity. Error estimates are obtained by a local least-squares reconstruction of the solution derivatives.[23,24] For the velocity field, the strain rate tensor is used for error estimation. An error estimate of the pressure solution is obtained by a local projection of the pressure field itself. Error estimates are obtained for the turbulence variables by projecting the finite element derivatives of $\mathcal{K}$ and $\mathcal{E}$ into a continuous field. An error estimate for the temperature is obtained in a similar fashion. Finally, an error estimate for the eddy viscosity is also constructed because slowly varying fields of $\mathcal{K}$ and $\mathcal{E}$ can result in rapid variation of the eddy viscosity. This is very important to the success of adaptation in turbulent flows because the eddy viscosity is the sole mechanism for diffusion of momentum and turbulence kinetic energy by turbulent fluctuations. See Refs. 7, 25, and 26 for examples and some discussions of these issues.

Once the error estimates are obtained for all variables, a better mesh must be designed. In our approach all variables are analyzed and contribute to the mesh adaptation process. For this an error estimate is obtained separately for each dependent variable. The mesh characteristics (element size) are derived for each variable on a given element. The minimum element size predicted by each of the dependent variable is selected on each element. Details of the steps of this algorithm are presented in references.[20,27]

Verification

The methodology is first validated on a problem possessing a closed-form solution. This problem is chosen so as to simulate a laminar round jet impinging on a heated flat plate. The exact solution is

$$u = 100x^2\left(e^{-x^2r^2} - e^{-0.01}\right)$$

$$v = -100xr\left(e^{-x^2r^2} - e^{-0.01}\right)$$

$$p = 1/[1 + 1000(r^2 + x^2)]$$

$$T = e^{400x/(1+4r^2)}$$

Appropriate source terms are obtained by substituting the preceding expressions into the Navier–Stokes and energy equations. The thermal boundary layer is much thinner than the velocity boundary layer. The temperature distribution is thus much more difficult to capture accurately than the velocity field. The geometry is illustrated in Fig. 1. The curved boundary corresponds to a streamline

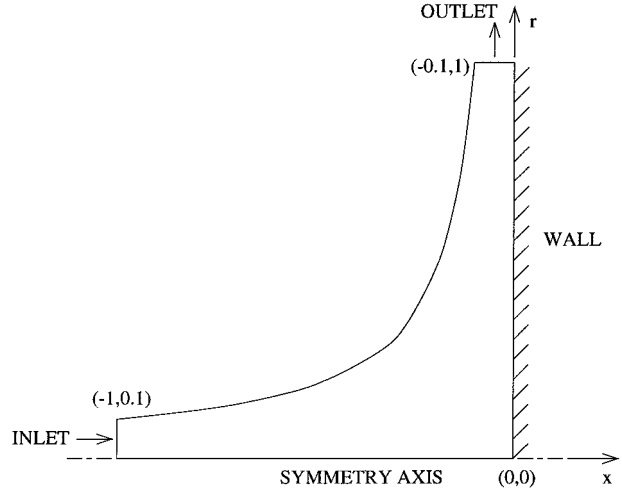

Fig. 1 Geometry for the analytical jet.

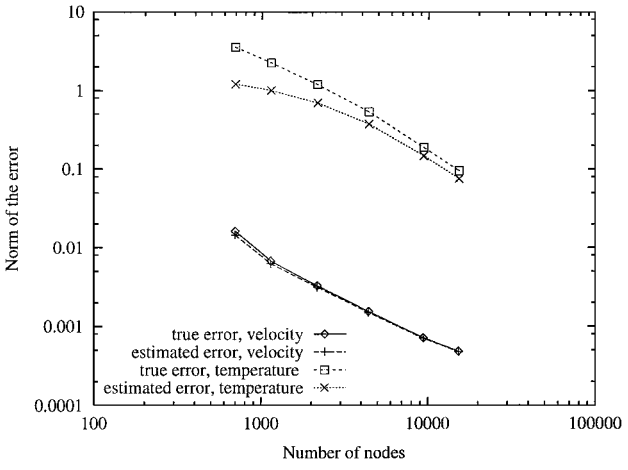

Fig. 2 Trajectory of the error for the analytical jet.

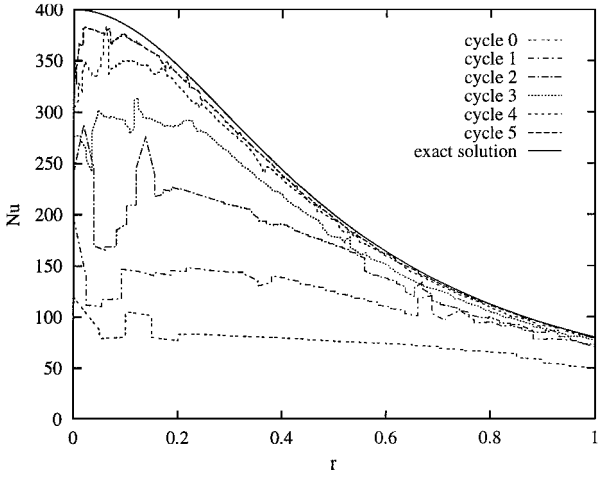

Fig. 3 Nusselt-number predictions for the analytical jet.

where the velocity vanishes. Symmetry conditions are applied at the bottom while Dirichlet boundary conditions are applied everywhere else. We set $Re = 50$ and $Pr = 0.7$.

The adaptive strategy is set to reduce the error by a factor 2 at each adaptive cycle (except for the last cycle, because of memory space constraints). Figure 2 shows the evolution of the error norms during the adaptive process. The norms used involve the first derivatives of the flow variables. Hence, this constitutes a demanding task. The error decreases with mesh refinement, and the numerical solution converges to the exact solution. The relative error (ratio of the norm of the error over the norm of the solution) is about 0.07% for the velocity and 1% for the temperature on the final mesh. Thus, the solution is very accurate even for derived quantities. As expected, the temperature gradient is less accurate than that of the velocity. Errors are plotted against the number of nodes because the mesh size is difficult to define precisely for unstructured meshes. The number of nodes behaves approximately as $1/h^2$. Hence, the observed unit slope in Fig. 2 agrees with the theoretical rate of convergence of two for quadratic elements. Finally, the error estimate is close to the true error. The finite element velocity appears to be in its asymptotic range of convergence on coarser meshes than temperature because it presents milder gradients than temperature. Moreover, most of the temperature error is located in the elements along the wall where the performance of the error estimator is known to be poorer. However, despite these observations, the accuracy of the error estimate improves as the mesh is refined.

The Nusselt-number distribution along the plate is shown in Fig. 3. The Nusselt number is defined as

$$Nu = q_w l/\lambda(T_w - T_\infty)$$

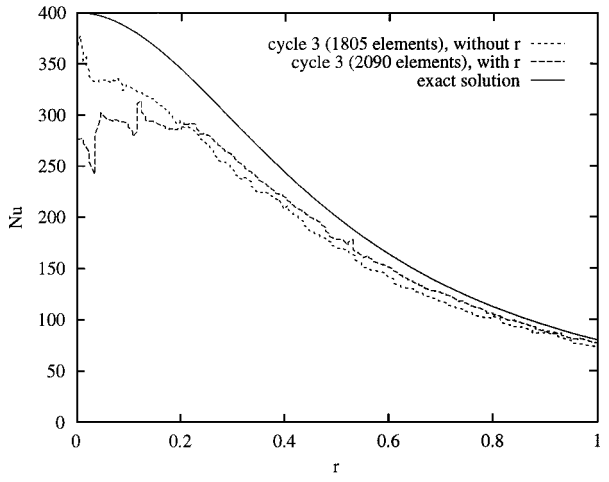

Fig. 4 Nusselt-number predictions: use of *r*.

where l is the characteristic length and T_∞ is the inlet temperature. Because the problem is solved in dimensionless form, Nu reduces to

$$Nu = \left.\frac{\partial T}{\partial x}\right|_{x=0}$$

Predictions on the first meshes are poor, but they improve with mesh refinement. The numerical solution clearly converges to the exact solution indicating that adaptivity can produce grid-independent solutions. The region near the symmetry axis ($r = 0$) experiences the largest errors. This is in part because of the extreme thinness of the thermal boundary layer in this region. However, there is another important cause to this behavior: the manner in which the error is distributed by the adaptive procedure. The transition operator attempts to equidistribute the norm of the error on each element. For axisymmetric problems the natural norm is of the form

$$\int \star\, r\, \mathrm{d}r\, \mathrm{d}x$$

The direct effect of the r in the norm is that errors located away from the axis weigh more heavily in the new mesh design than those located near the axis. Thus, if the error norm is equidistributed, the derivative Nu will be less accurate near the axis. In practice, one is interested in uniformly accurate values of the local Nusselt number. This is better achieved using a cartesian norm (without the r), which amounts more closely to equidistribution of the average pointwise error. Figure 4 compares the results obtained with or without the use of r in the norms of the error, on a typical intermediate adaptive cycle. As expected, the use of r generates solutions that are less accurate near $r = 0$ but more accurate farther away. Without the use of r, the elements generated near $r = 0$ are smaller, and the error is more uniformly distributed.

Computational verifications for turbulent cases with a closed-form solution can be found in Ref. 27.

Applications

Laminar Jet

The first application involves a laminar round jet impinging on a heated flat plate. The configuration corresponds to the experimental conditions of Scholtz and Trass.[28] The Reynolds number based on the inlet mean velocity and tube diameter is $Re = Ud/\nu = 950$, and the Prandtl number is 0.71 (air). The distance L between the jet lips and the wall is $2d$. The computational domain is shown in Fig. 5. It extends $20d$ from the axis in the radial direction and $3d$ upsteam of the jet lips. A parabolic (fully developped) velocity profile is assumed at the inlet. The wall is maintained at constant temperature.

The r was eliminated from the error norms because its wide range (from 0 to 20) is expected to cause accuracy problems near the axis as already demonstrated. The predicted distribution of the Stanton

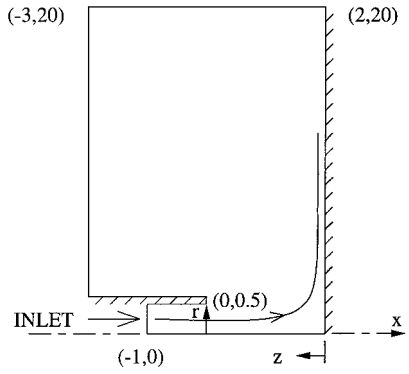

Fig. 5 Geometry for the laminar jet.

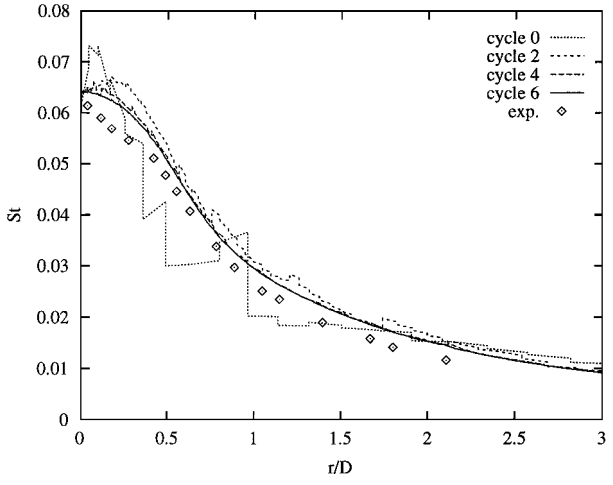

Fig. 6 Stanton-number predictions for the laminar jet.

number [$St = Nu/(Re\,Pr)$] is shown in Fig. 6. Predictions on the first mesh are irregular, oscillating, and inaccurate. However, as the mesh is refined, predictions converge to a single curve. The small differences between the last two meshes indicate that the solution is grid converged. Thus, the adaptive methodology is an efficient and straightforward way to perform grid-refinement studies and thus assess numerical accuracy. The solution appears to be uniformly accurate even near $r = 0$. This would not have been the case if the axisymmetric norm (with r) had been used.

Comparisons with experimental data show good agreement. The general behavior is reproduced. However, the global trend is an overprediction of the Stanton number. Other authors have reported similar observations. Saad et al.[29] report overpredictions almost everywhere, and Aihara et al.[30] overpredict St near the axis but underpredict it further away. Close examination of temperature contours by Aihara et al.[30] indicates that their first-order scheme suffers from excessive numerical diffusion. This reduces the Stanton number, especially far from the impingement region.

Figure 7 presents the predictions of the skin-friction coefficient C_f, defined as

$$C_f = \tau_w \big/ 0.5\rho U^2$$

In the present case this leads to

$$C_f = -\frac{2}{Re}\frac{\partial v}{\partial x}$$

Predictions on the initial mesh are poor but improve greatly as the mesh is refined. The differences in the final meshes are so small that we can conclude that the solution is grid independent and highly accurate, even for derived quantities such as C_f. No experimental data are available. However, predictions are compared with the numerical results of Deshpande and Vaishnav.[31] The results are similar.

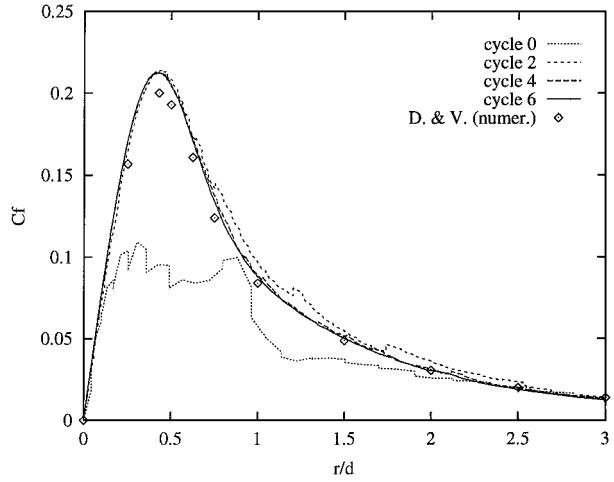

Fig. 7 Skin-friction predictions for the laminar jet.

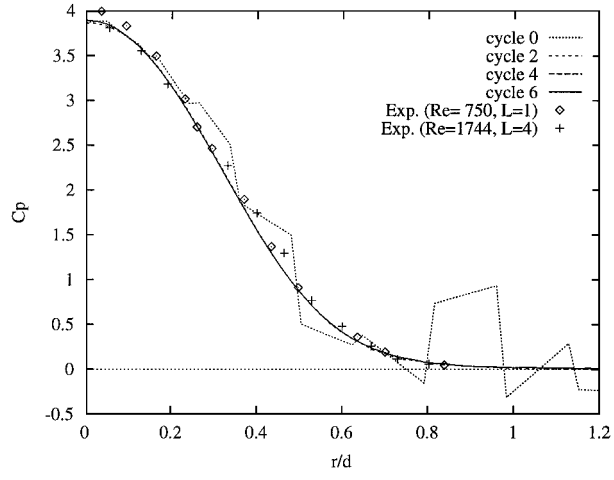

Fig. 8 Pressure coefficient predictions for the laminar jet.

As a final verification of convergence, Fig. 8 presents the distribution of the pressure coefficient C_p along the plate:

$$C_p = \frac{p - p_\infty}{0.5\rho U^2}$$

The solutions on the final meshes are clearly grid converged. Furthermore, convergence is faster for the presssure than for the derivatives of T or $\boldsymbol{u}$. This illustrates that the adaptive methodology is a useful tool to visualize and verify grid convergence. The numerical predictions are very close to the experimental data of Scholtz and Trass,[28] which are not exactly at the same conditions.

Turbulent Jet

We now turn our attention to a turbulent impinging jet. It has been repeatedly claimed that the k–ϵ model is deficient for this flow. In spite of this shortcoming, this severe test case serves to illustrate verification and validation exercices. The geometry is similar to the preceding case: the points (−3,20) and (2,20) are changed to (−2,5) and (2,5) (Fig. 5). The plate is located at a distance $L = 2d$ from the jet lips. The experimental data used for comparison are those provided at the 15th Meeting of the IAHR Working Group.[3] Because the flow data and temperature measurements are not exactly at the same conditions, two independent computations were made. The r is included in the definition of the error norm. This more traditional approach illustrates the effects of r. Also, the maximum value of r is lower than in the preceding case, and so its effect is expected to be less pronounced.

First, we consider the isothermal turbulent jet. The Reynolds number based on the inlet bulk velocity U and pipe diameter d is 23,000.

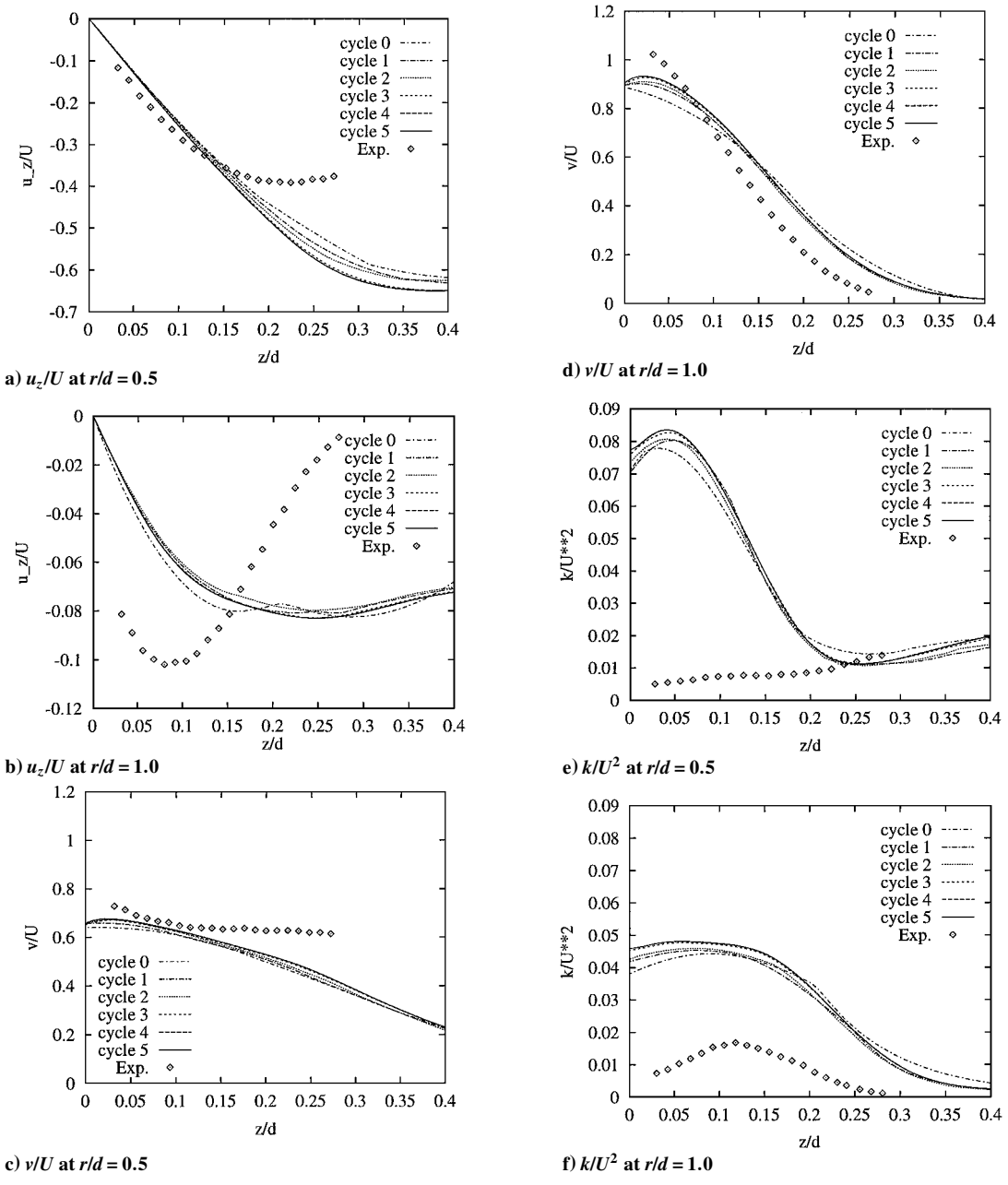

a) u_z/U at $r/d = 0.5$

b) u_z/U at $r/d = 1.0$

c) v/U at $r/d = 0.5$

d) v/U at $r/d = 1.0$

e) k/U^2 at $r/d = 0.5$

f) k/U^2 at $r/d = 1.0$

Fig. 9 Predictions of u_z/U, v/U, and k/U^2 for the turbulent jet.

Fully developed conditions, obtained in a separate computation, are imposed at the inlet. Adaptivity is set to reduce the error by a factor of 2 for $\boldsymbol{u}$, k, ϵ, and μ_T, except for the final mesh for which the reduction factor is set to 1.4.

Figure 9 compares predictions and measurements of u_z (the velocity component in the direction normal to the wall), v and k at two locations ($r/d = 0.5$ and 1.0). Predictions of v are fair, whereas those of u_z are poor. The predictions on k are much too high especially for $r/d = 0.5$. The k–ϵ turbulence model does not perform well for this type of problem. Other authors report similar observations.[3,5] Significant scatter is observed between predictions from various models and authors using the k–ϵ model always overpredict k by a similar amount. As seen in Fig. 10, k increases significantly near the impingement region, apparently as a result of a large value of the production term caused by the strong deceleration of the axial jet. Experiments indicate that k does not exhibit such an increase along the symmetry axis close to the wall.[4] Behnia et al.[5] suggest a modified turbulence model to alleviate this nonphysical production of turbulence. Their model performs better for both flow and turbulence quantities. However, the degree of generality of their model is somewhat restricted. A crucial point here is that grid convergence is achieved. The curves clearly overlap on each other as the mesh is refined. The small differences between last cycles confirm grid convergence. One can say that a numerically exact solution of the equations has been achieved, or in other words that the predictions are verified. On the basis of such verified results, validation of turbulence models is rigorous.

Inspection of Fig. 9 raises the issue of the positioning of the computational boundary with wall functions. The question is this: should we really displace the numerical boundary by a distance y? Yes seems to be a logical answer because it agrees with theory and is closer to the physics. However, it is not always easy to proceed to such a displacement, and many authors just ignore it. The consequences of this choice are more important if comparison with experimental data is confined to a small region close to the wall, which is the case here. The displacement distance is $y = 0.04$, which represents 10% of the observation zone. The results presented are not corrected to account for this distance. Nonzero values of v and

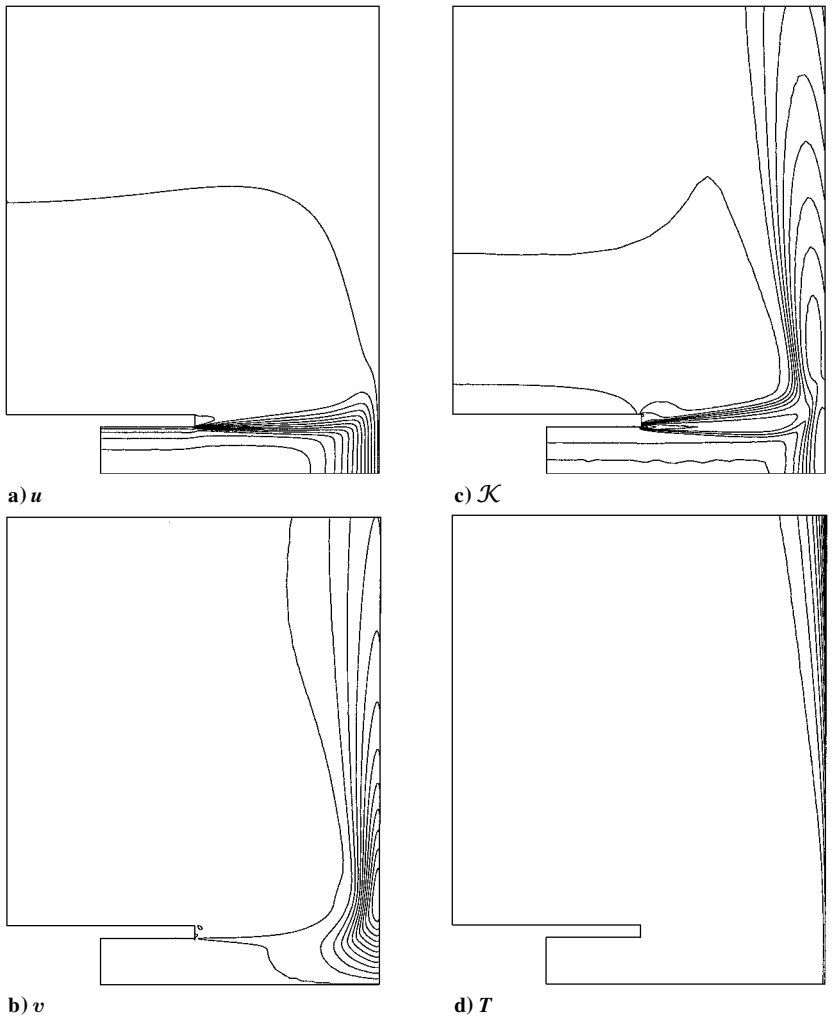

Fig. 10 Solution on final mesh for the turbulent jet.

k at $z = 0$ are nonphysical. But imposing $u = 0$ at a distance y will also yield nonphysical results, especially here where u reaches high values. There is also an issue in terms of mass conservation in the zone covered by wall functions. In this case the numerical results would be farther from the experiments if we consider a displacement. Clearly, the use of wall functions is simple but not perfect. Furthermore, wall functions were not typically designed for flows that are not parallel to walls.

We now turn our attention to the case when the preceding jet is heated. A constant heat flux is applied at the wall. The Reynolds number is 2.375×10^4, and the Prandtl number 0.71. The geometry is the same as in the isothermal case except that the inlet tube thickness is $t/d = 0.132$ instead of $t/d = 0.031$. The adaptive strategy is set to reduce the error by a factor of 1.667 between each adaptive cycle.

Figure 10 presents contours of the solution on the final mesh. The smoothness of the contour lines provides a visual cue of the accuracy of the solution. Notice how the jet hits the wall and is deviated radially. The radial velocity reaches its maximum near $r/d = 0.9$ and then decreases. High levels of turbulence and severe fronts of $\mathcal{K}$ are present in the shear layer where turbulence production is important. The displayed contours are those of the computational variable $\mathcal{K}$. The correspondence to k is direct. Finally, the thermal boundary layer is very thin, especially near the symmetry axis. However, it grows in the radial direction. As can be seen in Fig. 11, the mesh is well adapted to the solution: it is refined where the solution gradients are large. Notice the refinement along the wall, in the shear layer emanating for the lips, and in the regions where the jet turns into a radial wall jet.

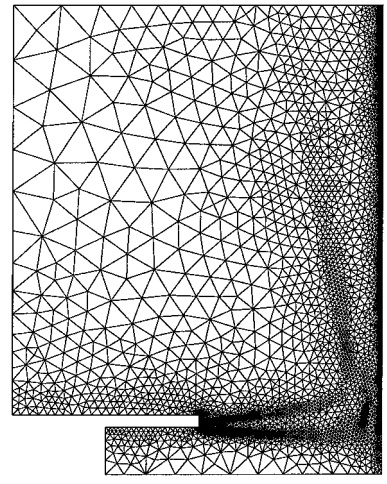

Fig. 11 Final mesh for the turbulent jet.

Predictions of the local Nusselt number [$Nu = q_w d/\lambda(T_w - T_\infty)$] are shown in Fig. 12. The heat flux q_w is known (it is imposed), and the temperature of the wall T_w (the real wall, not the numerical boundary) is computed using wall functions. Predictions clearly collapse to a single curve as the mesh is adaptively refined. The solution is thus grid converged and numerically accurate. In this case the only source of inaccuracy is that of the prediction of the wall temperature. When the wall temperature is imposed instead of

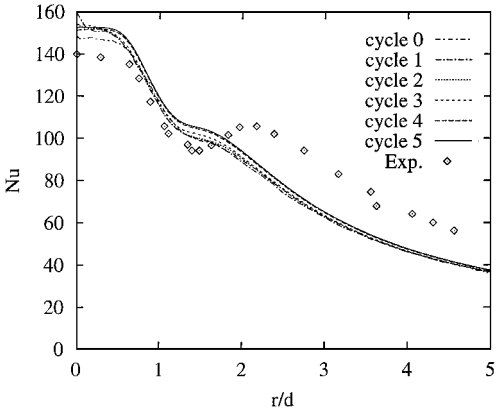

Fig. 12 Nusselt-number predictions for the turbulent jet.

a heat flux, the computation of *Nu* involves the evaluation of the temperature gradient, which is less accurate than the temperature itself. In such a case grid convergence of *Nu* looks much more like the one shown in Fig. 3.

The discussion would not be complete without comparisons with the experimental data of Baughn and Shimizu[32] and other numerical results. For $r/d < 2$ the numerical prediction of *Nu* is above and close to the experimental data, say within about 10%. The secondary maximum near $r/d = 2$ is not reproduced. Farther away, *Nu* is underpredicted. The code N3S developed at Électricité de France delivers very similar results with the same turbulence model and wall functions.[3] Craft et al.[6] studied the performance of four turbulence models. Some of them reproduce the local extremum, but they all overpredict *Nu* for low values of r and sometimes much more so than the present results. Behnia et al.[5] obtain somewhat better results with their V2F model. They also illustrate the bad performance of the low-Reynolds-number k–ϵ model, which overpredicts the stagnation Nusselt number by as much as 170%. They even state that the standard k–ϵ model used with wall functions excessively overpredicts the stagnation Nusselt number, but provide no detail or numerical result to support their assertion. We have shown here that wall functions used with mesh adaptation perform reasonably well for heat transfer predictions, even if the flow is not parallel to the wall. The overprediction of the stagnation Nusselt number seems to be related to too high a level of turbulence kinetic energy. The underprediction further away from the axis may be a consequence of the upstream overprediction of k and the underprediction of v. Globally, the results are fair. It would have been surprising to obtain an excellent agreement for heat transfer given the poor predictions of the flow and turbulence fields.

Conclusions

An adaptive finite element algorithm was applied to laminar and turbulent jet impingement heat transfer. Turbulent flow simulations use the standard k–ϵ model and wall functions. Computations on an analytical laminar jet confirm the good performance of the methodology in terms of accuracy and error estimation capabilities. For the laminar jet the methodology produces grid-independent solutions in a few cycles. Predictions are in agreement with measurements.

The turbulent impinging jet is a more complex flow and is more difficult to predict. However, grid independence is still achieved with the adaptive methodology, allowing a rigorous evaluation of the validity of the model. For this problem the performance of the k–ϵ turbulence model is poor when the verified predictions are compared with experimental data, especially for the prediction of k. More sophisticated turbulence models should be used to obtained more realistic results, even if heat-transfer predictions have shown to be fair when using the k–ϵ model with wall functions. Predictions of the Nusselt number are much better than one would have expected given the poor accuracy of the flow and turbulence quantities.

In general, the adaptive methodology is a powerful approach to handle such complex heat transfer problems and to generate accurate solutions to the differential equations modeling the flow. The methodology provides control and quantification of the error. It also provides visual cues of grid convergence and accuracy of the numerical solutions.

Acknowledgments

This work was supported in part by NSERC, FCAR, and AFOSR Grant F49620-96-1-0329.

References

[1]Turgeon, É., and Pelletier, D., "Effects of Adaptivity on Various Finite Element Schemes for Turbulent Heat Transfer and Flow Predictions," *Numerical Heat Transfer—Part A*, Vol. 38, 2000, pp. 847–868.

[2]Launder, B. E., "Current Capabilities for Modelling Turbulence in Industrial Flows," *Applied Scientific Research*, Vol. 48, No. 3–4, 1991, pp. 247–269.

[3]Brison, J. F., and Brun, G., "Round Normally Impinging Turbulent Jets," 15th Meeting of IAHR Working Group on Refined Flow Modelling, École Centrale de Lyon, France, Oct. 1991.

[4]Cooper, D., Jackson, D. C., Launder, B. E., and Liao, G. X., "Impinging Jet Studies for Turbulence Model Assessment—I. Flow-Field Experiments," *International Journal of Heat and Mass Transfer*, Vol. 36, No. 10, 1993, pp. 2675–2684.

[5]Behnia, M., Parneix, S., and Durbin, P. A., "Prediction of Heat Transfer in an Axisymmetric Turbulent Jet Impinging on a Flat Plate," *International Journal of Heat and Mass Transfer*, Vol. 41, No. 12, 1998, pp. 1845–1855.

[6]Craft, T. J., Graham, L. J. W., and Launder, B. E., "Impinging Jet Studies for Turbulence Model Assessment—II. An Examination of the Performance of Four Turbulence Models," *International Journal of Heat and Mass Transfer*, Vol. 36, No. 10, 1993, pp. 2685–2697.

[7]Pelletier, D., and Ilinca, F., "Adaptive Remeshing for the k–ϵ Model of Turbulence," *AIAA Journal*, Vol. 35, No. 4, 1997, pp. 640–646.

[8]Ilinca, F., and Pelletier, D., "Positivity Preservation and Adaptive Solution for the k–ϵ Model of Turbulence," *AIAA Journal*, Vol. 36, No. 1, 1998, pp. 44–51.

[9]Ilinca, F., Pelletier, D., and Garon, A., "An Adaptive Finite Element Method for a Two-Equation Turbulence Model in Wall Bounded Flows," *International Journal for Numerical Methods in Fluids*, Vol. 24, No. 1, 1997, pp. 101–120.

[10]Ignat, L., Pelletier, D., and Ilinca, F., "A Universal Formulation of Two-Equation Models for Adaptive Computation of Turbulent Flows," *Computer Methods in Applied Mechanics and Engineering*, Vol. 189, No. 4, 2000, pp. 1119–1140.

[11]Pelletier, D., Hétu, J.-F., and Ilinca, F., "Adaptive Finite Element Method for Thermal Flow Problems," *AIAA Journal*, Vol. 32, No. 4, 1994, pp. 741–747.

[12]Pelletier, D., Ilinca, F., and Hétu, J.-F., "Adaptive Finite Element Method for Convective Heat Transfer with Variable Fluid Properties," *Journal of Thermophysics and Heat Transfer*, Vol. 8, No. 4, 1994, pp. 687–694.

[13]Pelletier, D., and Ilinca, F., "An Adaptive Finite Element Method for Mixed Convection," *Journal of Thermophysics and Heat Transfer*, Vol. 9, No. 4, 1995, pp. 708–714.

[14]Pelletier, D., Ignat, L., and Ilinca, F., "Adaptive Finite Element Method for Conjugate Heat Transfer," *Numerical Heat Transfer—Part A*, Vol. 32, No. 3, 1997, pp. 267–289.

[15]Pelletier, D., Ilinca, F., and Turgeon, É., "An Adaptive Finite Element Method for Forced Convection," *International Journal for Numerical Methods in Fluids*, Vol. 25, No. 7, 1997, pp. 803–823.

[16]Ignat, L., Pelletier, D., and Ilinca, F., "An Adaptive Finite Element Method for Turbulent Forced Convection," *Numerical Heat Transfer—Part A*, Vol. 34, 1998, pp. 847–871.

[17]Ilinca, F., and Pelletier, D., "Adaptive Finite Element Solution of Compressible Turbulent Flows," *AIAA Journal*, Vol. 36, No. 12, 1998, pp. 2187–2194.

[18]Launder, B. E., and Spalding, D. B., *Mathematical Models of Turbulence*, 6th ed., Academic Press, London, 1972.

[19]Arpaci, V., and Larsen, P., *Convection Heat Transfer*, Prentice–Hall, Upper Saddle River, NJ, 1984.

[20]Ilinca, F., "Méthodes d'Éléments Finis Adaptatives pour les Écoulements Turbulents," Ph.D. Dissertation, Mechanical Engineering Dept., École Polytechnique of Montréal, April 1996.

[21]Crouzeix, M., and Raviart, P. A., "Conforming and Non-Conforming Finite Element Methods for Solving the Stationary Stokes Equations," *RAIRO-Numerical Analysis*, Vol. 3, No. 1, 1973, pp. 77–104.

[22]Peraire, J., Vahdati, M., Morgan, K., and Zienkiewicz, O. C., "Adaptive Remeshing for Compressible Flow Computations," *Journal of Computational Physics*, Vol. 72, No. 2, 1987, pp. 449–466.

[23]Zienkiewicz, O. C., and Zhu, J. Z., "The Superconvergent Patch Recovery and a Posteriori Error Estimators. Part 1: The Recovery Technique," *International Journal for Numerical Methods in Engineering*, Vol. 33, No. 7, 1992, pp. 1331–1364.

[24]Zienkiewicz, O. C., and Zhu, J. Z., "The Superconvergent Patch Recovery and a Posteriori Error Estimators. Part 2: Error Estimates and Adaptivity," *International Journal for Numerical Methods in Engineering*, Vol. 33, No. 7, 1992, pp. 1365–1382.

[25]Ilinca, F., Pelletier, D., and Garon, A., "An Adaptive Finite Element for a Two-Equation Turbulence Model in Wall Bounded Flows," *International Journal for Numerical Methods in Fluids*, Vol. 24, No. 1, 1997, pp. 101–120.

[26]Ilinca, F., Pelletier, D., and Arnoux-Guisse, F., "An Adaptive Finite Element Scheme for Turbulent Free Shear Flows," *International Journal of Computational Fluid Dynamics*, Vol. 8, No. 3, 1997, pp. 171–188.

[27]Turgeon, É., "Application d'une Méthode d'Éléments Finis Adaptative à des Écoulements Axisymétriques," M.S. Thesis, Mechanical Engineering Dept. École Polytechnique de Montréal, June 1997.

[28]Scholtz, M. T., and Trass, O., "Mass Transfer in a Non Uniform Impinging Jet, Part 1 & 2," *AIChE Journal*, Vol. 16, No. 1, 1970, pp. 82–96.

[29]Saad, N. R., Douglas, W. J. M., and Mujumdar, A. S., "Prediction of Heat Transfer Under an Axisymmetric Laminar Impinging Jet," *Industrial and Engineering Chemistry Fundamentals*, Vol. 16, No. 1, 1977, pp. 148–154.

[30]Aihara, T., Kim, J., and Maruyama, S., "Effects of Temperature-Dependent Fluid Properties on Heat Transfer due to an Axisymmetric Impinging Gas Jet Normal to a Flat Surface," *Warme- und Stoffubertragung*, Vol. 25, No. 1, 1990, pp. 145–153.

[31]Deshpande, M. D., and Vaishnav, R. N., "Submerged Laminar Impingement on a Plate," *Journal of Fluid Mechanics*, Vol. 114, Jan. 1982, pp. 213–236.

[32]Baughn, J. W., and Shimizu, S., "Heat Transfer Measurements from a Surface with Uniform Heat Flux and an Impinging Jet," *Journal of Heat Transfer*, Vol. 111, No. 4, 1989, pp. 1096–1098.